NASA-CR-194274

DIST. CATEGORY UC-63
DOE/JPL-955843/84/12
DRD No. SE5
DRD No. 139

LARGE-AREA SHEET TASK
ADVANCED DENDRITIC WEB GROWTH DEVELOPMENT

C. S. Duncan, R. G. Seidensticker, and J. P. McHugh

Annual Report

October 23, 1982 to October 22, 1983

January 13, 1984

Contract No. 955843

CONTENTS

3

LIST OF FIGURES

1. SUMMARY

The thermal models used for analyzing dendritic web growth and calculating the thermal stress were reexamined to establish the validity limits imposed by the assumptions of the models. Also, the effects of thermal conduction through the gas phase were evaluated and found to be small. New growth designs, both static and dynamic, were generated using the modeling results. Residual stress effects in dendritic web were examined. In the laboratory, new techniques for the control of temperature distributions in three dimensions were developed. A new maximum undeformed web width of 5.8 cm was achieved. A 58% increase in growth velocity at 150 μm thickness was achieved with dynamic hardware. The area throughput goals for transient growth of 30 and 35 cm^2/min were exceeded.

2. INTRODUCTION

Silicon dendritic web is a single-crystal silicon ribbon material which provides substantial advantages for the low-cost manufacture of solar cells. Growth from a melt of silicon without the use of constraining dies is a significant feature of the process, which results in an oriented single-crystal ribbon having excellent surface characteristics. In common with other more typical processes such as Czochralski growth, impurity rejection into the melt permits the use of less pure "solar grade" starting material without significantly affecting cell performance. A unique property of the dendritic web process is the growth of long ribbons of controllable width and thickness, which not only facilitates automation of subsequent processing into solar cells, but also results in high material utilization since cutting and polishing are not required.

On the present contract, three broad areas of work are emphasized:

1. The development of thermal stress models in order to understand the detailed parameters which generate buckling stresses, and the application of these models to the development of new low-stress design concepts.

2. Experiments to increase our understanding of the effect of various parameters on the web growth process and to complement and verify the results of the modeling effort.

3. The construction and utilization of an experimental web growth machine which contains in a single unit all the mechanical and electronic features developed previously so that experiments can be carried out under tightly controlled conditions.

2

The principal objective of this work has therefore been to expand our knowledge and understanding of both the theoretical and experimental aspects of the web growth process to provide a solid base for substantial improvements in both area throughput and web crystal quality, and to develop the tools necessary to carry out this objective.

During this reporting period, the thermal models were used to generate new low-stress growth configurations. Techniques and hardware were developed to generate improved temperature distributions in the growth system. Significant demonstrations included the area throughput goals for transient growth of 30 and 35 cm^2/min, a new maximum web width of 5.8 cm, and a 58% improvement in growth velocity at standard thickness using dynamic growth configurations.

7

3. TECHNICAL PROGRESS

3.1 Modeling and Material Analysis

3.1.1 Introduction

The modeling and material evaluation activities during the past year can be grouped in three main catagories: 1) model evaluation and modification, 2) design of new configurations, and 3) evaluation of residual stress in dendritic web ribbons. The first area, model evaluation and modification, includes a critique of the inherent limitations of the existing models, especially the model for buckling evaluation. The results indicate that the existing models are adequate for present studies, but that certain modifications might well be made if more accurate calculations are required for very wide web growth. In addition, the possibility was investigated for including thermal conduction through the furnace gas in the ribbon temperature model. It was concluded that the heat transfer via gas conduction is so small relative to the radiative heat transfer that it would be inappropriate to modify the existing model at this time.

The second area, design of new growth configurations, considered both the design of very low-stress configurations for wide growth and the design of dynamically trimmed configurations for fast growth. Several design guidelines were identified for low-stress systems and appropriate hardware was fabricated. Parametric analysis identified LIN (the position of the growth interface with respect to the bottom of the crucible lid) as the most sensitive parameter for controlling speed and again, experimental configurations were made to dynamically vary this factor.

The final area covered in this section concerns the residual stress observed in dendritic web crystals. The interpretation of split width measurements is reviewed and interpreted in terms of the real stress fields in the web crystals.

3.1.2 Evaluation of Stress and Buckling Models

During development of the models for calculating the thermal stresses and buckling of dendritic web crystals, the model predictions were tested as often as possible against the observed behavior of real systems. The validity of the modeling seemed to be established by the excellent agreement of the predicted critical buckling dimensions for the J98M3A configuration and the observed web dimensions for which buckling actually occurred. The comparison is shown in Figure 1, where the solid represents the calculated boundary between flat and buckled ribbon and the points represent the observed width and thickness at which deformation actually occurred. With the development of improved, low-stress growth systems such as the J460, web crystals have been grown at widths that significantly exceed the predictions of the buckling analysis at normal thicknesses, although the agreement is much better for thin web crystals which buckle at relatively narrow widths. We have reexamined the assumptions and application of the stress and buckling models to see why the buckling calculations might become conservative when applied to wider web growth.

One of the principal assumptions implicit in both the thermal stress and the buckling calculations is the validity of the use of a finite ribbon segment (finite element mesh) to represent the properties of a semi-infinite ribbon (web crystal). Furthermore, in the application of the model to parametric studies in which the ribbon width is varied, the total length of the mesh has been maintained at ten centimeters so that the aspect ratio of the ribbon segment becomes smaller for wide web. This would obviously become a problem in the extreme case of the segment length equal to its width since then a semi-infinite ribbon would be represented by a square plate. It was the

5
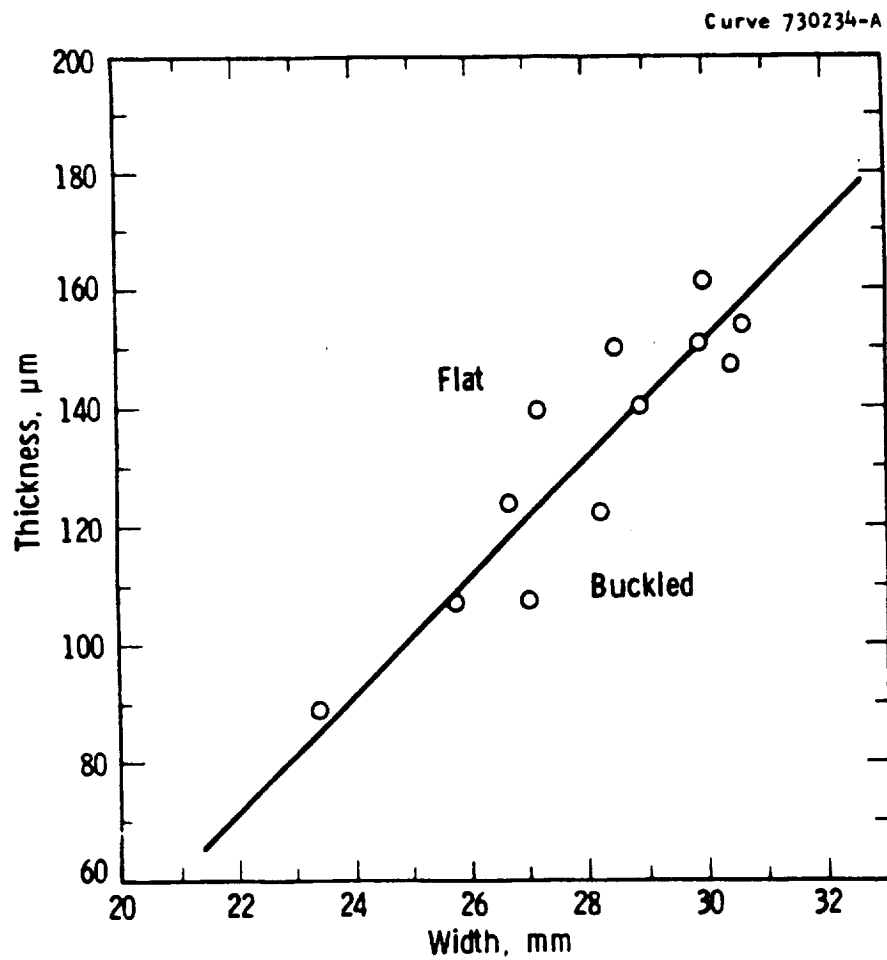
Figure 1. Buckling width versus thickness for J98M3A configuration.
Solid curve is the calculated dependence and the points are
observed values.

6

purpose of the present work to establish at least a qualitative
evaluation of the application limits of the present model configura-
tion. Each of the three models, temperature, stress, and buckling, was
examined to see what effect the width of the ribbon segment might have
on the validity of the results.

3.1.2.1 Temperature Model

The input data for all the stress calculations is a temperature
profile along the length of the web and the model, the calculations of
which have been discussed at length elsewhere.[1] Since only a one-
dimensional temperature distribution is used in our present analyses,
the width of the ribbon is immaterial. However, should modeling of
ribbon segments longer than ten centimeters eventually be considered,
then the alternate numerical integration routines included in the code
may be required to provide reliable temperature data at larger distances
from the growth front. For our present purpose, however, the
temperature profile model can be dismissed as being pertinent to whether
a narrow or a wide web is being modeled.

3.1.2.2 Stress Model

One of the principal assumptions of both the stress and the
buckling models is the use of a finite ribbon segment (finite element
mesh) to represent the semi-infinite web crystal. The principal effect
of the finite segment in the stress analysis arises from the boundary
conditions that are used for the end of the segment which should be
"attached" to the balance of the ribbon. The two conditions most easily
accommodated by the finite element code are: 1) a "free" boundary so
that the longitudinal stress σ_x and the shear stress σ_{xy} are both zero
on the boundary or 2) a constant displacement u_x on the boundary. The
effect of the "free" boundary condition has been discussed
previously[2]; briefly, it was found that the stress distributions are
perturbed for a distance approximately equal to the ribbon width. A
similar effect occurs when the constant displacement condition is

7

imposed, but in that case the stresses are increased rather than nulled at the boundary. The two effects are shown in Figure 2 for the longitudinal stress on the axis of a 2.7 cm ribbon. Also shown in the figure is an approximate evaluation of the stress derived from the Boley and Wiener series solution[3]

$$\sigma_x = \frac{E}{6} (w^2 - 3y^2) (\alpha T)''$$ (1)

By ten centimeters from the growth front, the temperature is varying slowly enough so that the approximate solution should be quite good, and while neither boundary condition gives results that agree with the series solution, the free boundary ($\sigma_x(10) = 0$) is probably a better choice. For meshes wider than about four centimeters, however, the boundary effect would become much more serious and a longer mesh segment should be used. For the present purposes, the effect is probably tolerable for a four centimeter wide model; and more importantly, it would underestimate the stresses and thus underestimate the tendency of the ribbon to buckle.

3.1.2.3 Buckling Model

There are two aspects of the use of the buckling model itself which could lead to a conservative prediction of the tendency for a ribbon to deform. One is related to the size (aspect ratio) of the finite element mesh and the other to the interpolation/extrapolation law assumed in the analysis of the results.

The effect due to the mesh size is the neglect of the stiffening contribution from the ribbon adjacent to the segment being modeled. Physically, a growing crystal would be deformed over a much larger length than the 10 cm segment being modeled; however, the mathematics of the model do not consider the increase in internal energy associated with that deformation. To some extent this neglect is compensated for by neglecting the thermal strain energy as well, but the degree of compensation is affected by the details of the stress distribution. For
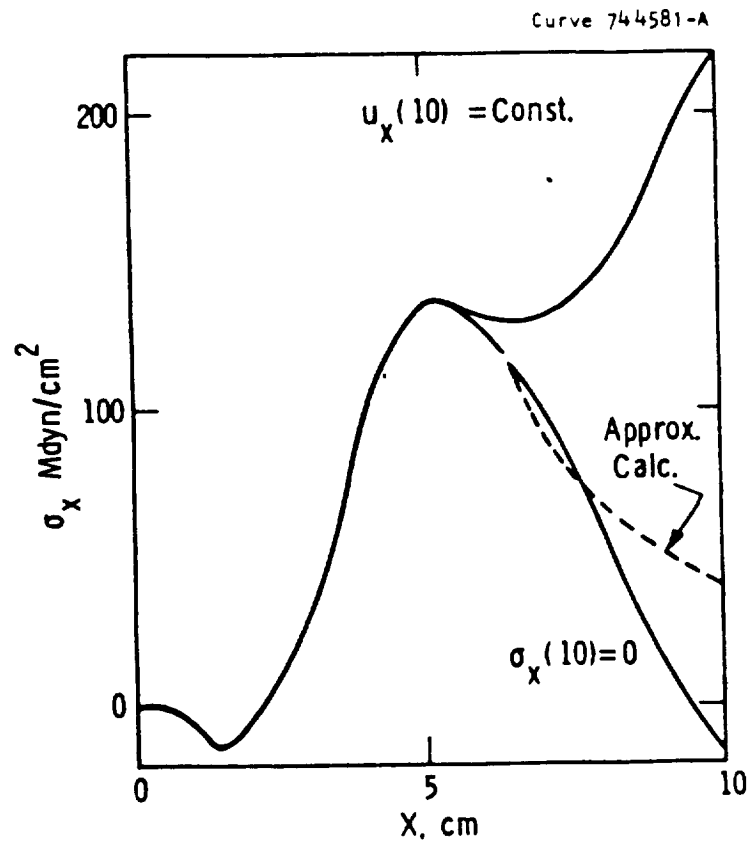
Figure 2. Effect of boundary conditions at x = 10 on σ_x along the ribbon centerline.

9

example, in some earlier, relatively high-stress configuration such as the J98M3A, the major stress peak was large and relatively close to the growth front, as shown in Figure 3. Further, buckling occurred at the relatively narrow width of about 2.7 cm for 150 μm thick ribbon. For this case, the buckling predictions were in very good agreement with the observed growth behavior. Further, model length effects were checked for a similar configuration (the J181) and found to be negligible. Increasing the segment length by 30 percent gave only a one percent increase in the buckling eigenvalue, well within the uncertainty of the numerical technique.[4]

In the case of the J460, however, the stiffening effect may be more pronounced. As seen in Figure 3, the major stress peak is smaller and further from the interface. Furthermore, a buckling calculation at 3.95 cm gave an eigenvalue of 1.04, indicating that deformation was imminent. Also, with a eigenvalue so near unity, interpolation errors should be negligible. Nevertheless, actual growth experience indicates that ribbons up to about 4.9 cm wide and 150 μm thick can be grown from the configuration without deformation, so that the calculation is obviously conservative. Neglect of the extra stiffening from the balance of the ribbon seems a reasonable cause for this variance between calculation and observation and should be even more pronounced for the ultra-low stress J483.

Once the results of a buckling model are available, there is a final step in the procedure which involves the interpretation of the analysis. In general, the combination of the thermal profile and the ribbon dimensions will not be "critical"; that is, it will be safely in the flat regime of growth, or perhaps it should have buckled. The particular state of affairs can be described in terms of the eigenvalue λ in the equation

$$[K] \ \{\Delta\} = \lambda \ [S] \ \{\Delta\} \qquad (2)$$

where $[K]$ is a stiffness matrix which depends on the ribbon dimensions

10

Figure 3. Delta x-stress calculated for the J98M3, the J460, and the J483 growth configurations.

and elastic constants, [S] is the initial stress matrix resulting from
the imposed thermal field, and {Δ} the (unknown) deviation from
flatness. The eigenvalue λ is in effect a multiplier which can be
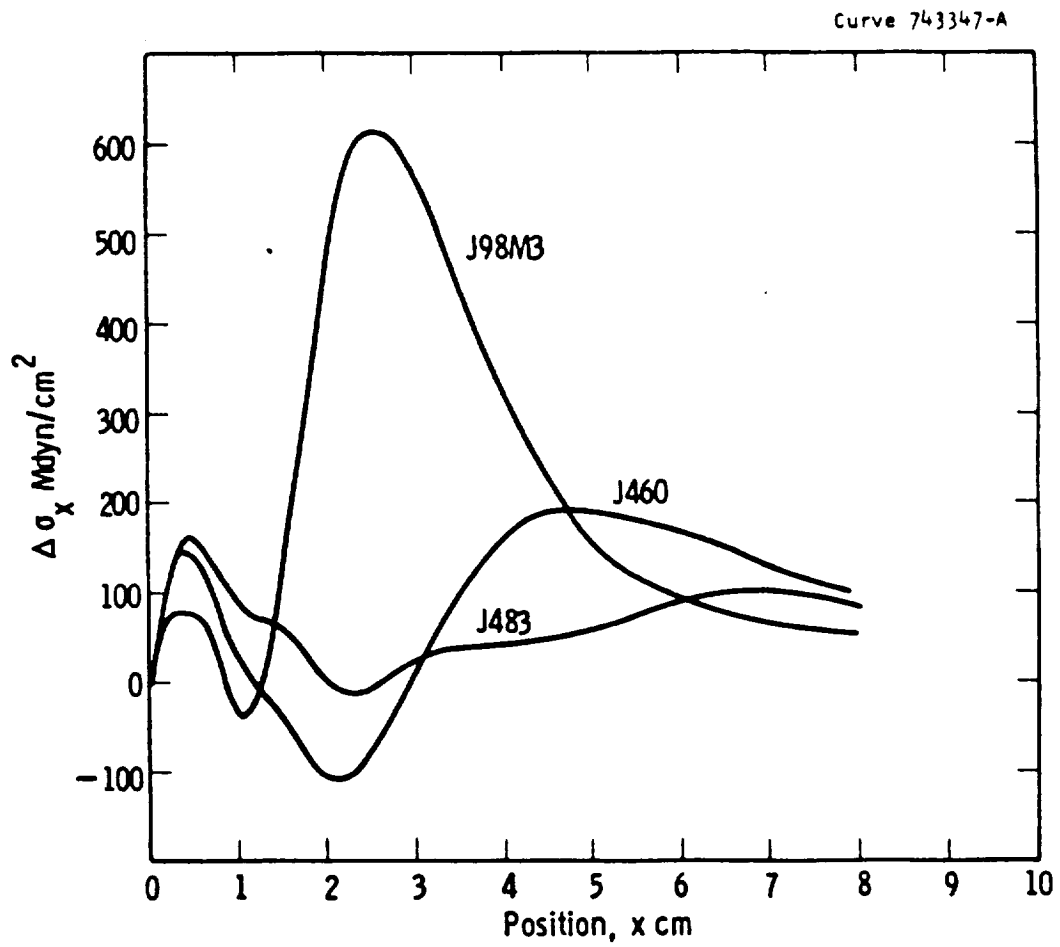applied equally to <u>all</u> the stress components at each node of the mesh.
If $\lambda<1$, then the ribbon would have buckled; if $\lambda>1$, then the ribbon
would be flat under the assumed conditions. The critical part of
interpreting the buckling results is to determine the critical ribbon
dimensions for which $\lambda = 1$.

During the development of the model, buckling calculations were
run for a number of ribbon widths using temperature data for the rela-
tively high-stress J181 configuration.[5] From the results it was found
that λ varied approximately as $W^{-3.63}$, and this interpolation/
extrapolation law has been used since then for other configurations. It
is useful to note that the stiffness, [K], should vary about as W^{-2} and
that the "far" $\Delta\sigma_x$ peak at about 5 cm, shown in Figure 4, of the stress
distribution varies about as $W^{1.6}$. These two exponents would combine to
give the $W^{-3.6}$ dependence found for λ. The $\Delta\sigma_x$ parameter is, however,
only one measure of the stresses present in the system. If the stresses
were independent of the ribbon width, which is a reasonable approximation
for the stress peak at about 1 cm, then one might expect λ to vary as
W^{-2}. Other components of the stress field have other width dependences
generally much less than $W^{1.6}$.

When very low-stress configurations are analyzed, $\lambda\gg1$ even at
the 3.95 cm width. Since wider width modeling is suspect, for the
reasons just discussed, extrapolation must be used to determine the
critical width. For example, the model of the J483 yielded $\lambda = 1.848$ for
3.95 cm web 150 µm thick. On the basis of $W^{-3.63}$, this would imply that
$\lambda = 1$ at 4.68 cm, but on the basis of W^{-2}, then $\lambda = 1$ at $W = 5.37$ cm.
In the case of ribbons 300 µm thick, $\lambda = 4.662$ and the corresponding
critical widths are 6.0 cm and 8.5 cm for the two extrapolation laws.
In reality, the critical width should lie between these two values.
However, in these cases, the ribbon-stiffening effect has not been
considered and hence even wider widths should be realized in practice.
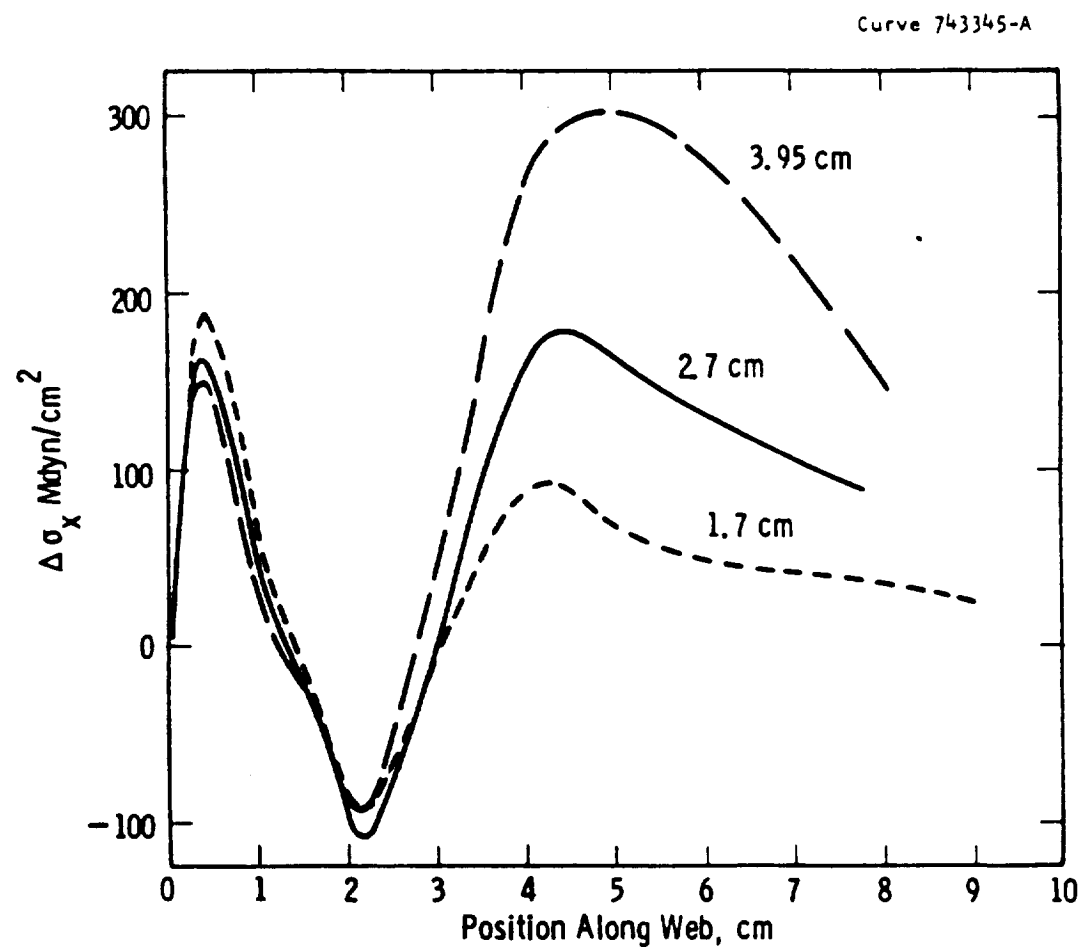
Figure 4. Delta x-stress calculated for the J460 configuration at ribbon widths of 1.7, 2.7, and 3.95 cm.

3.1.2.4 Conclusions

The three component models used for buckling analysis have been examined to find reasons why the model predictions might be conservative. The most likely reason appears to lie in the buckling model. As very low-stress configurations are analyzed, wider ribbon segments have been used without concommitant increase in segment length, and as a result, the model becomes a somewhat less accurate representation of the semi-infinite ribbon. The situation could be improved by, for example, doubling the length of the ribbon segment being analyzed, a relatively minor change in the stress or buckling models. In the case of the temperature model which provides the initial input data, improvement in the integration procedure would be required, a more than trivial effort. Furthermore, we can make a rough estimate of the degree to which the critical buckling width may be underestimated based on the empirical data on the J460 configuration. Thus, the present methods of analysis are reasonably serviceable for our present purposes.

One final aspect of the buckling model should be discussed; namely, the type of deformation which is considered: symmetric (bowing) or antisymmetric (twist). Both types can be modeled and both types have been observed in actual growth. In practice, however, the symmetric or bowing deformation is the most frequently observed with low-stress configurations and most frequently serves to terminate the growth of wide web material. In some situations, the growing crystal will actually snap back and forth between the front and the back of the growth slot in response to attempts to realign it with the web guides. On the basis of these observations, the symmetric buckling case is usually modeled and is the model case which generally agrees with observations, as in Figure 1.

3.1.3 Gaseous Conduction Effects in the Temperature Model

The computer program which is used to calculate the temperature profile in the growing crystal only considers radiative heat transfer

between the ribbon and its surroundings. In principle, other mechanisms such as conductive and convective heat transfer in the gas phase could be included; however, some estimate to the magnitude of these mechanisms is required to justify the added complexity of the model. Convective transfer is beyond the scope of the present program; conductive effects are the subject of this section.

An initial estimate of the importance of gas conduction can be made by comparing conductive transfer with radiative transfer in a critical region of the ribbon. For the present case, we will examine the effects in the first few millimeters above the growth front. The geometry for the analysis is shown in Figure 5. By virtue of the design (J483 configuration, model case 9-53), the only elements "seen" by the ribbon at the growth front are the outside ambient (300^OK). The radiative interchange with each element can be evaluated from the equation[6]

$$\dot{q} = \varepsilon\sigma \ (T^4-T_i{}^4) \ \ f_i(\theta) \tag{3}$$

where $\dot{q}$ is the radiative heat interchange per unit area, ε is the emissivity (.6), σ the Stefan-Boltzmann constant (5.67×10^{-12} w/cm^{2}K^4), T the absolute temperature of the ribbon, and T_i the temperature of the ith element. The angular view factor $f(\theta)$ is given by[6]

$$f(\theta) = sin\theta_{i2} \ - \ sin\theta_{i1} \tag{4}$$

where θ_{i1} and θ_{i2} are the subtending angles with respect to the web surface normal for the ith element.

Similarly, the gaseous heat conduction per unit area (from both sides of the web) can be estimated by the simple conduction equation

$$\dot{q}(gas) = 2k_g(T - T_i)/\ell \tag{5}$$

where k_g is the thermal conductivity of the gas and ℓ is the

15
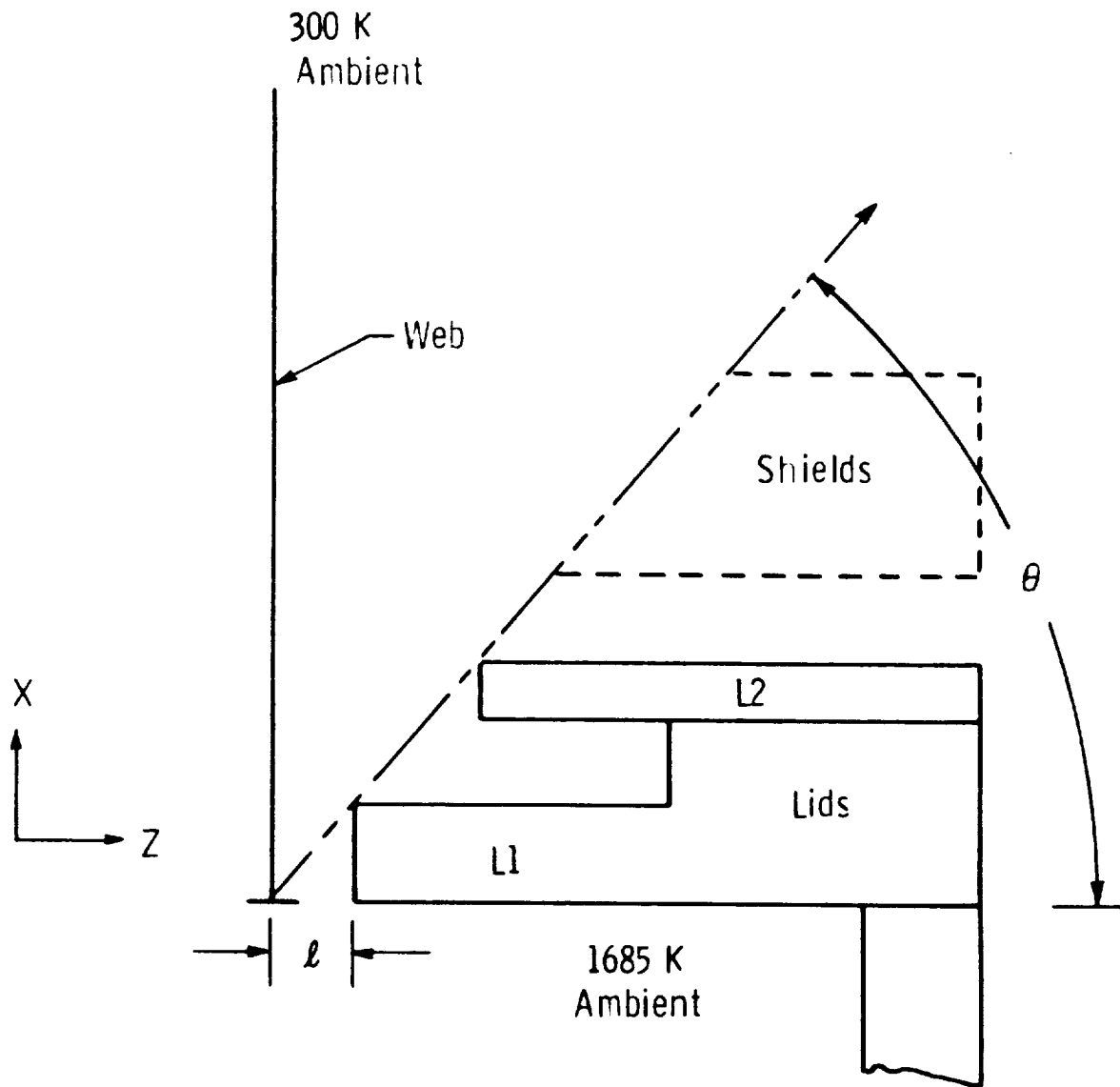
Figure 5 -- Geometry for gaseous conduction effects.

20

perpendicular distance from the point on the web to the ith element. Using 5.56×10^{-4} w/cm-K for the conductivity of argon at 1685°K,[7] a distance of $\ell = .3$ cm, $T-T_i = 95^{O}$K, and $\dot{q} = .35$ w/cm^2. Table 1 compares the various heat-transfer quantities for the ribbon element at the interface (T = 1685°K), and it can be seen that at the interface thermal conduction changes the total heat transfer by only about 4%. Consideration of the geometry and the web temperature profile suggests that this is the location where the effect would be the largest and, on the basis of the present data, the gas conduction is too small to warrant including in the model.

Table 1

Heat-Transfer Quantities at the Interface (T = 1685°K)

Element	Element Temperature ^{O}K	$f(\theta)$	$\dot{q}$ W/cm^2	
Cavity	1685	1	0	
Lid 1	1590	.785	4.459	
Lid 2	1585	.082	.489	
Ambient	300	.133	3.644	
Total Radiative Transfer			8.592	
Estimated Gas Transfer			.352	3.9%
Total			8.944	

3.1.4 New System Designs

Design work for new dendritic web growth system has been directed toward two principal areas: growth systems producing small buckling stress to facilitate the growth of wider ribbon crystals and growth systems which could be modified during operation (dynamically trimmed) for greater throughput. Design guidelines were developed for both types of systems and prototype systems were proposed.

21

3.1.4.1 Low Buckling Stress Systems

Previous work in the development of growth systems for wide crystals has suggested that the critical conditions for deformation of a growing web ribbon are related to a longitudinal stress (σ_x) peak that occurs several centimeters above the growth front. This peak, in turn, could be related to a similar peak in the $(\alpha T)''$ characteristic of the temperature profile in the web. Hence, the design philosophy for reducing the tendency for deformation in wide crystals was to modify the temperature profile to reduce the critical $(\alpha T)''$ peak. A guide to the design of hardware which would achieve this goal was found in the observation that this peak occurred where the ribbon emerged from the shield stack and, further, that the height of the peak diminished as the height of the shield stack increased.

Following these design guides, a growth system (now known as J483) was modeled which had a lid/shield stack almost 6 cm tall. The $(\alpha T)''$ characteristic of the temperature profile is shown in Figure 6. The effects of the individual lower elements (lids, shields, spacers) is evident in the first few centimeters; at higher positions the individual element contributions are too small to be resolved.

The stress calculations based on the same temperature profile as Figure 6 confirmed the anticipated low-stress magnitudes. One of the critical stress parameters, $\Delta\sigma_x$ $[\sigma_x(\text{center})-\sigma_x(\text{edge})]$, has been plotted for the J483 geometry in Figure 3 (Section 3.4.2); also shown are similar curves for the J98M3A and the J460 geometries. It is readily apparent that the stress calculated for the J483 is significantly less than for the J460 configuration, the best of the prior designs. Both the J460 and the J483 have similar stress peaks in the first centimeter or so, which is reasonable since the lid design is the same for both cases. Further up the ribbon, however, the stress maxima are about 190 Mdyn/cm^2 for the J460 but only 93 Mdyn/cm^2 for the J483.

The y-stress distribution also tends to be a maximum near the growth front as shown in Figure 7. Again, this distribution is very
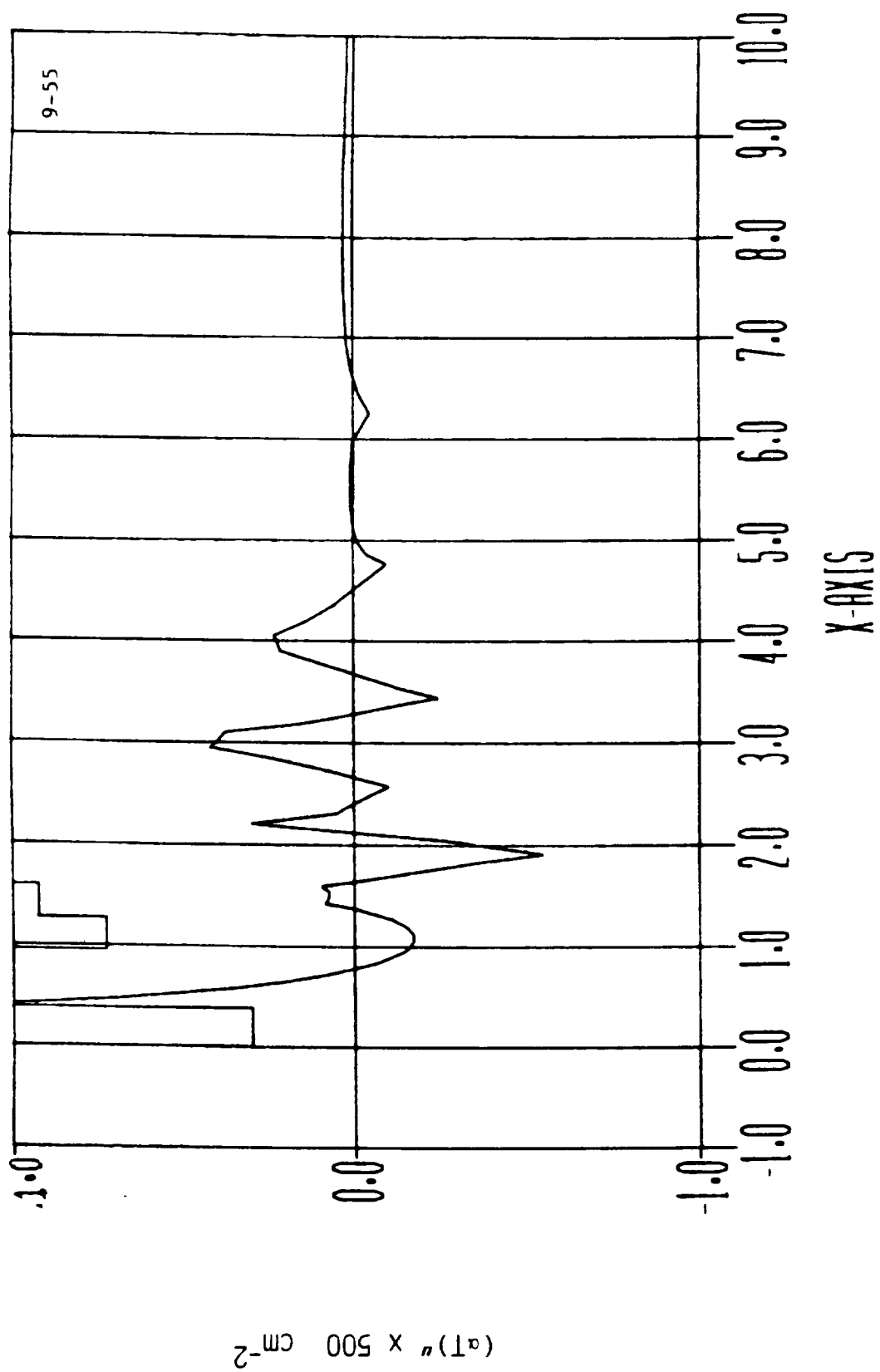
Figure 6 -- $(\alpha T)''$ versus position along ribbon for the J483 configuration.
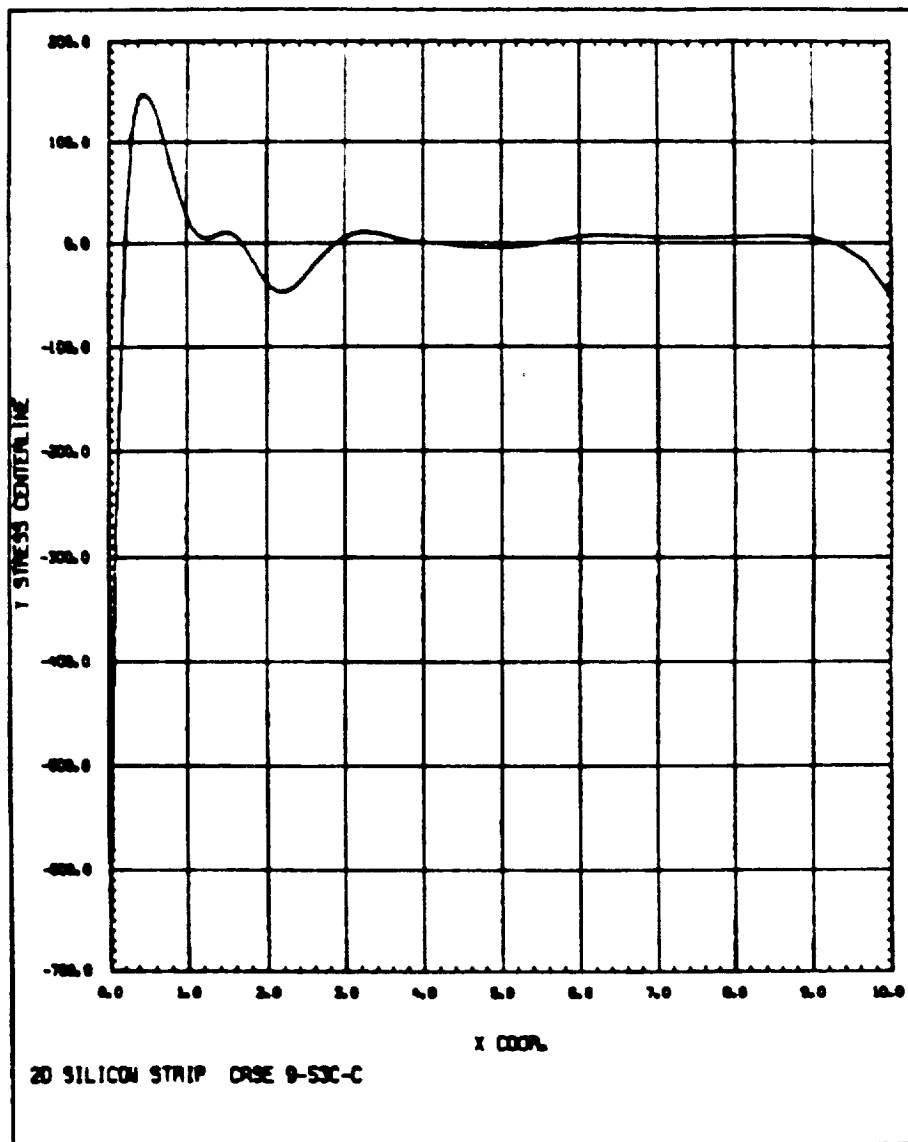
Figure 7 -- Centerline y-stress versus position along the ribbon length for J483 configuration.

similar to the corresponding curve for the J460 design. In fact, the
magnitude of the maxima and minima in the curve are generally somewhat
less than in the J460 case. As yet, an extensive comparison of residual
stress data for the J460 and the J483 is not available; however,
preliminary residual stress data suggest that the y-stress should be at
an acceptable level in the J483 design.

When buckling calculations were run on this configuration, the
resulting eigenvalues suggested that flat crystals in the 6 to 7 cm
range should be possible. For such wide, low-stress material, however,
the assumptions of the buckling analysis became less applicable (see
Sections 3.1.2) and the ultimate ribbon width must be validated by
experiment.

3.1.4.2 Dynamic Growth Configurations

The second area of growth system design was concerned with
systems that could be modified during the growth of a dendritic web
crystal. The concept of the dynamic growth system was based on the
proposition that optimum conditions for initiating growth may not be
optimum for high throughput of an already growing crystal, and that
overall better growth might be obtained if the growth configuration
could be changed while the crystal was growing.

Parametric studies using the temperature and stress models
indicated that there was very little that could be usefully done by
modifying the shield temperatures, slot widths, etc. The position of
the growth front with respect to the bottom of the lid, the LIN
parameter (shown in Figure 8), had a pronounced effect on the growth
speed, however, which made it a prime candidate for dynamic variation
during growth.

It has long been known that changes in melt height have signifi-
cant effects on web growth, especially in the velocity required to
maintain a constant thickness of the ribbon. Early work with
modeling[8] suggested that melt height changes could also influence the

21

26
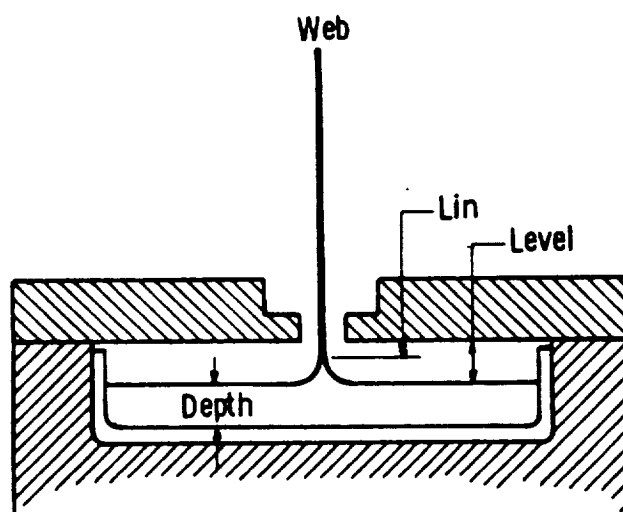
Figure 8 -- Melt geometric parameters.

22

residual stresses in the material, and some experimental data tended to confirm this observation. Recently, however, more sophisticated growth systems have been developed within which the melt level effects on stress are not quite as obvious, although the influence on growth velocity at constant thickness is still significant. Following this current experimental lead, modeling work was done to investigate the effect of melt level within current growth configurations such as the J460.[9]

Chosen for study was the standard J460 growth configuration, shown schematically with the resulting $(\alpha T)''$ curve in Figure 9 (taken from Ref. 9); the concomitant delta x-stress curve is shown as the curve LIN = 0 in Figure 10. Additional modeling runs were then made for this configuration with the interface 1 and 2 mm (LIN = 0.1, 0.2 cm) below the bottom of the lid. It was found that the changes in the delta x-stress were negligible, the main effect being a slight shift of the stress curve corresponding to the shift in the position of the growth front. If, as suspected, the delta x-stress is a good measure of the driving force for ribbon buckling, then changes in the melt height should have little if any effect on the deformation of the web.

The changes in the y-stress components near the interface are more evident but still relatively small. The three cases are shown in Figure 11, where it can be seen that as the melt level falls (LIN increases), the y-stress on the ribbon centerline decreases slightly and the maximum value at about 0.5 cm also decreases. Although the visco-elastic deformation process is too complex for a detailed prediction of the resulting residual stress, intuitively it would appear that the lower melt levels would produce lower stresses. Inspection of the curves in Figure 11 shows that, while there is some difference between the three cases, the differences in fact are relatively minor, and it may be that the resulting stress differences will be too small to be clearly evident in the material measurement. In fact, the J460 material that has been evaluated all shows very low residual stress, and

23
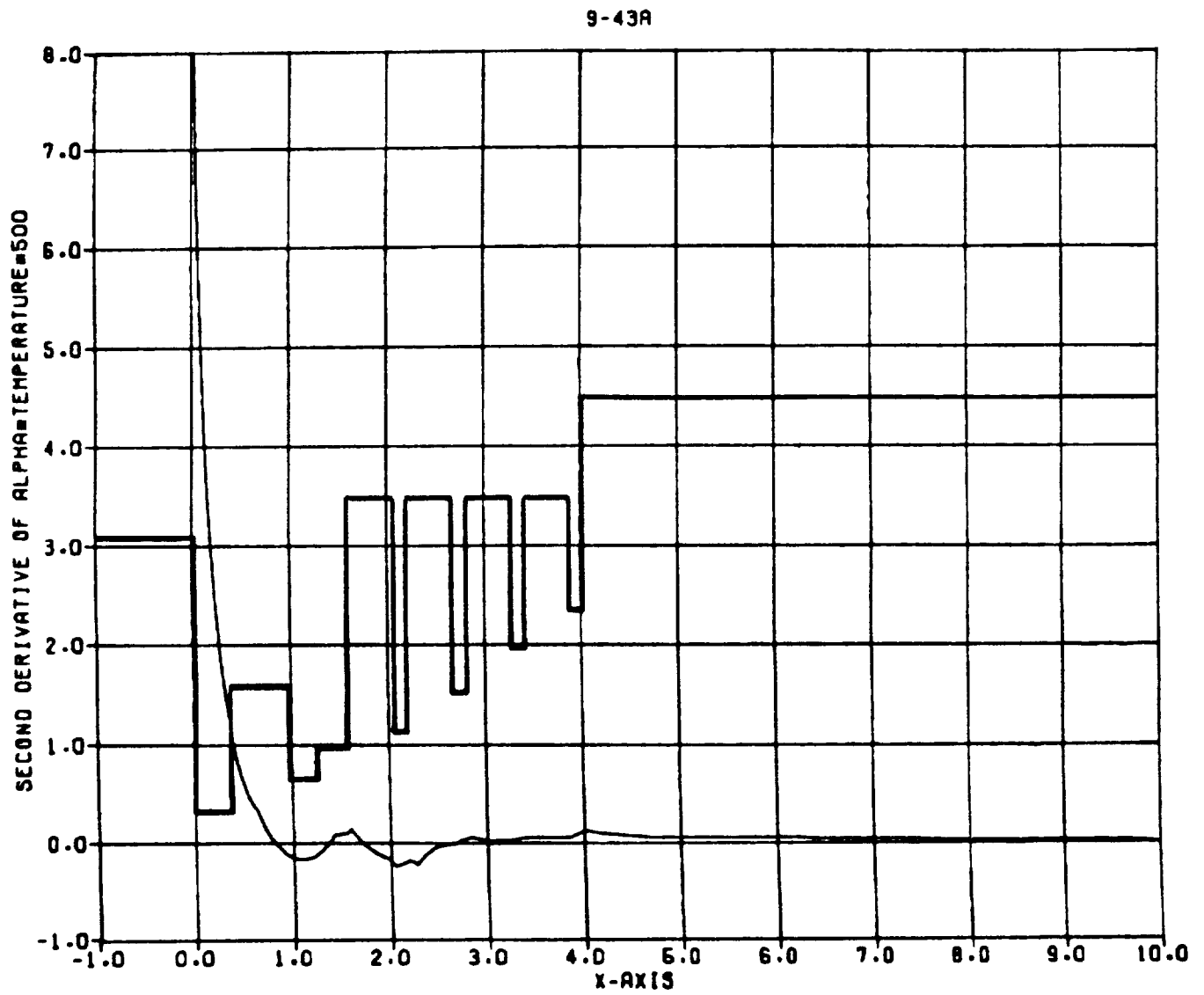
Figure 9 -- Temperature profile results for J460 configuration.

24
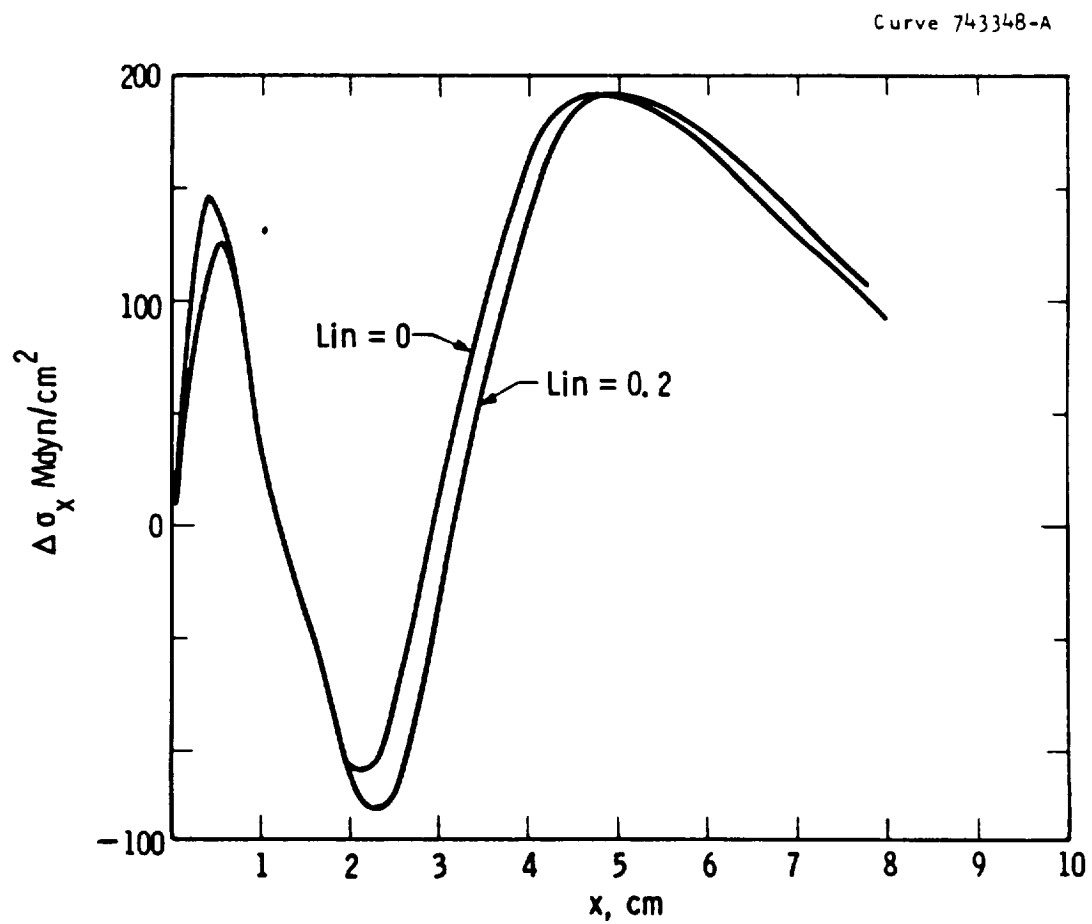
Figure 10 -- Delta x-stress versus position for J460 configuration;
curves are for different interface position (LIN).

29
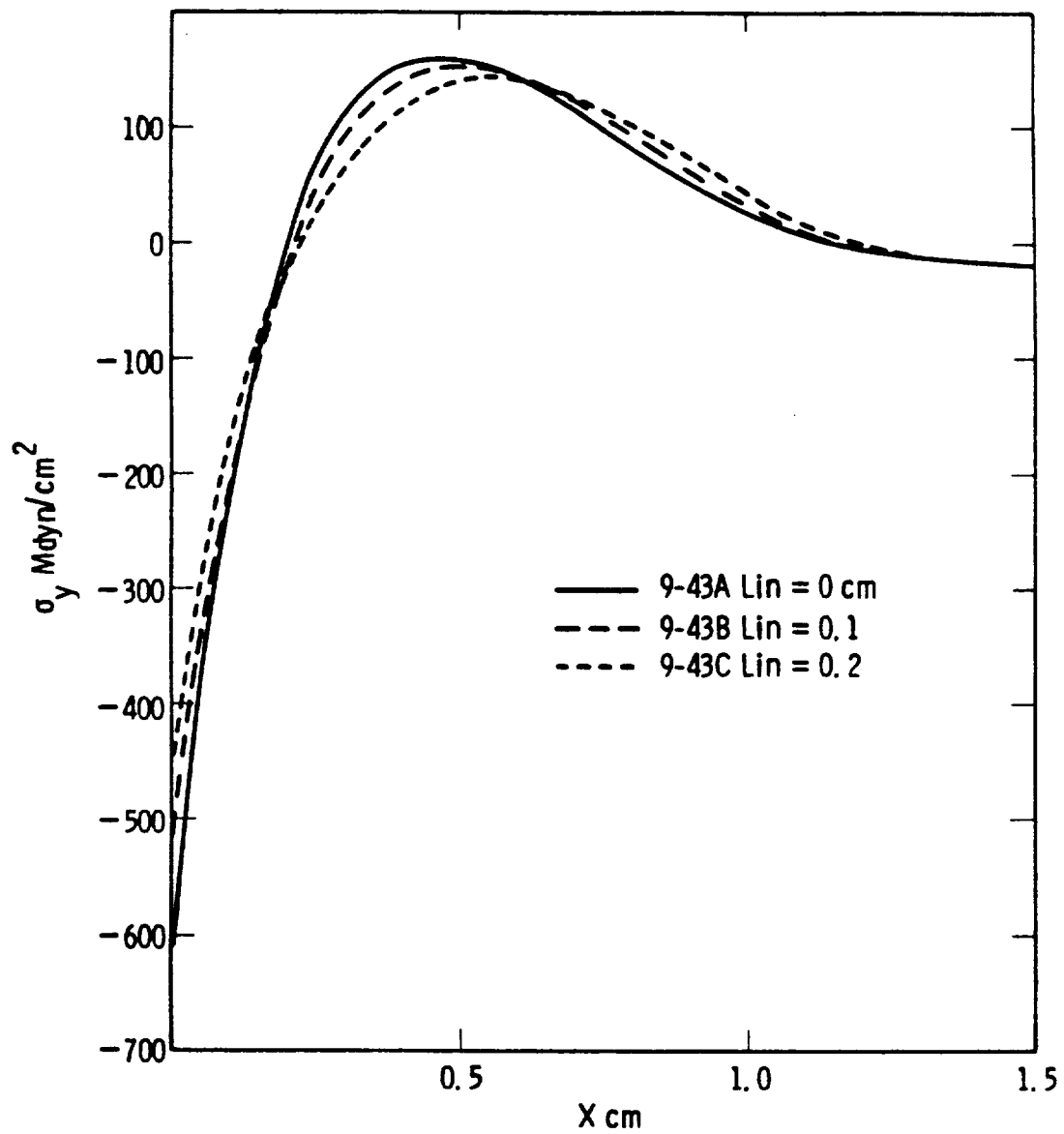
Figure 11 -- Y-stress versus position -- J460 configuration.

30

differences between material grown at high melts and that grown at low melts are small.

The major differences between the high melt (LIN = 0) and the lower melts (LIN = 0.1, 0.2) show up in the velocity effect, as seen in Figure 12. The web partial velocity, V_w, changes from 1.52 cm/min (LIN = 0) to 1.18 cm/min at LIN = 0.2; a similar, although much smaller, decrease occurs in the melt contribution to the velocity. The net result is that changing the melt level (growth without replenishment) drastically affects the attainable velocities for web growth. On the other hand, the result shows that the melt height can be used as an adjustable thermal parameter; growth could be initiated at a lower melt level where seeding seems to be easier, and then the melt level gradually increased to allow a relatively fast speed for steady-state growth.

3.1.5 Residual Stress Studies

One of the parameters which can be used to evaluate the quality of dendritic web crystals is the residual stress present in the ribbons. Although a residual stress field must exist in those crystals which have buckled or otherwise show some permanent deformation, we shall for the present purposes only consider the residual stresses in that material which is macroscopically flat and straight. From a practical viewpoint, such residual stress has not generally been considered deleterious unless it was large enough to interfere with the handling of the crystals, or unless the associated dislocations have degraded the electrical quality of the silicon. Neither situation has been a serious concern for several years.

Our renewed interest in the residual stress of dendritic web crystals arises from the potential of using the parameter as a measure of the thermal stress conditions near the growth front in a growing crystal. The propensity of a growing crystal to deform apparently provides a measure of the stresses away from the growth front, and residual stress can serve the same diagnostic function near the freezing

31
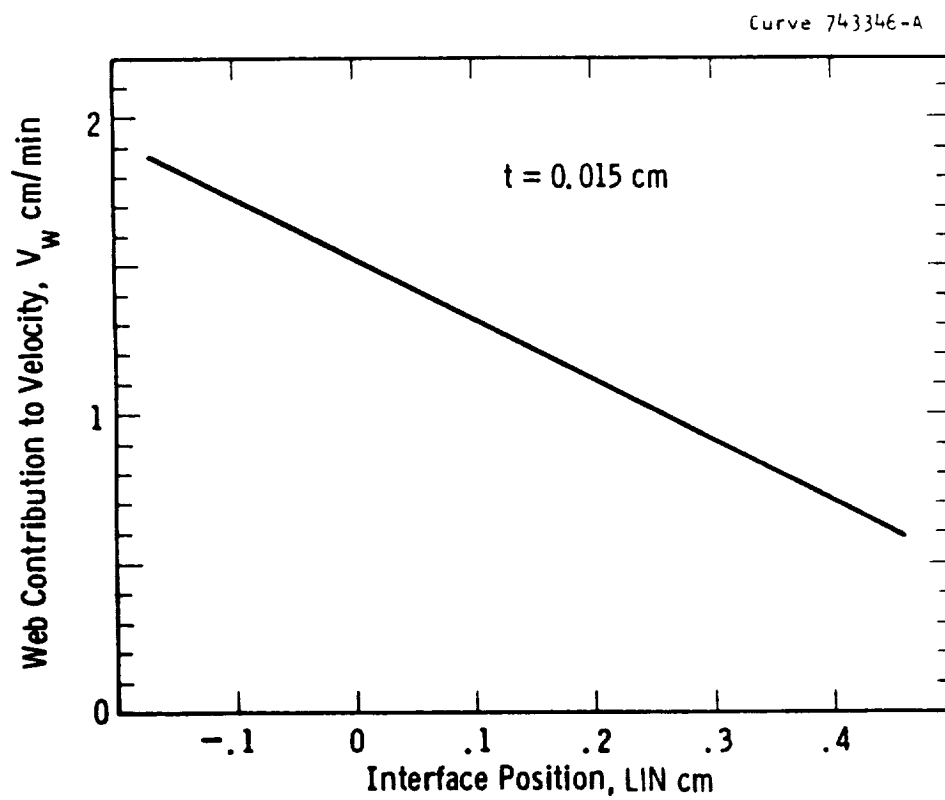
Figure 12 -- Variation of the web contribution to growth velocity with interface position (LIN).

28

interface. Although the actual magnitude of the residual stresses is small, they appear to be a characteristic of the specific growth configuration and even of the growth conditions, e.g., coil position, melt height, and possibly even the convective flow of the furnace gas near the crystal. Furthermore, it now seems appropriate to consider the possible interaction of the residual stress fields with the thermal stresses. Our stress modeling has so far assumed an elastic medium, an assumption justified on the basis that the measured residual stresses have been very small compared to the calculated thermal stresses. With advanced growth systems, however, the thermal stresses have been reduced to a magnitude where the observed residual stresses could be as much as 10 or even 20% of the elastic thermal stresses. Under such conditions, a somewhat more careful consideration of the residual stress seems warranted.

In our laboratory, residual stress in a web crystal has been defined operationally in terms of the curvature of the split in a ribbon which has been fractured down its centerline (see Appendix 1). The "residual stress" in the crystal has then been taken as the surface (or edge) stress resulting when a similar (half) strip was bent to the same curvature. This parameter has been useful as a semiquantitative measure of the suitability of the material for device fabrication: above about 80 Mdyn/cm^2 (8 MPa, 1184 psi), the material may be difficult to handle without danger of spontaneous fracture and would be considered highly stressful; below about 10 Mdyn cm^2, the material would be "low stress"; below about 2 Mdyn/cm^2, the uncertainty of the technique, the material would be "zero stress." While such measurements and definitions are useful for the classification of the material and for evaluation of the growth systems, it tends to obscure the fact that the actual stress in the crystal is a spatially dependent tensor.

In fact, the situation is somewhat simpler than it might be. Measurements made at intervals along a long web crystal indicate that the stress or, more properly, the curvature, is essentially constant so that

29

$$\frac{\partial}{\partial x} (\sigma_{ij}) = 0. \tag{6}$$

For the plane stress case with constant curvature (for wide webs the bounding dendrites have a negligible contribution to the moment of inertia), equilibrium considerations require that the stress field have only a σ_x component, which can vary across the width of the strip, i.e., only $\sigma_x(y) \neq 0$.

In the half ribbon, this stress distribution will give rise to a bending moment[10]

$$M = \int y\sigma_x dA. \tag{7}$$

The equivalent counter moment, if applied externally, would be simply

$$M = CIE \tag{8}$$

where C is the curvature (C = a2 in our analysis; Appendix 1), I is the moment of inertia defined by

$$I = \int y^2 \, dA \tag{9}$$

and E is Young's modulus. Using this notation and assuming a uniform flat strip, the maximum equivalent stress would be simply

$$\sigma(max) = M \frac{w/2}{I} . \tag{10}$$

This $\sigma(max)$ is the number which we have been using for the "residual stress."

The real residual stress distribution in a web crystal could be calculated by making a series of split width measurements on a sample in which a narrow strip is removed from the edge between measurements. The change in moment would then give the true residual stress in the strip removed from the ribbon. Some preliminary measurements on web measured

30

with and without dendrites indicate that the real stresses are similar in magnitude to the "residual stress" defined by Equation 10.

3.2 Experimental Web Growth

3.2.1 Introduction

The experimental work during this period encompassed a variety of areas, including: 1) the evaluation of new low-stress growth configurations, 2) the development of a width-limiting version of the low-stress J460 design, 3) the development of dynamic configurations for the control of the interface-to-lid distance, 4) the development of techniques for improved control of lateral temperature distributions in the growth systems, and 5) the systematic collection of system temperature and melt level data. During the course of these efforts, we were able to demonstrate: 1) steady-state web growth, 2) area throughputs exceeding the contract goals of 30 and 35 cm^2/min for transient growth, 3) a new maximum crystal width of 5.8 cm, and 4) a growth velocity of 3.0 cm/min at 150 µm thickness.

3.2.2 System Measurements

Two types of system measurements were made routinely during growth runs: top shield temperatures and melt level. Some lid temperature measurements were also made, but not on a regular basis. These measurements serve two purposes: 1) to provide input data for and to verify the results of the modeling effort; and 2) to enable us to correlate growth characteristics, such as the thickness-velocity relationship, with system temperatures and interface position.

Top shield temperatures were measured with type-K thermocouples cemented into small holes drilled partially through the shields close to the edge of the slots. Thermocouple outputs were fed into a datalogger which prints out the shield temperatures as desired. Temperatures are recorded at "hold" and "grow." Temperatures were measured as a function

31

35

of coil height and shield spacing. In most runs, temperature data were obtained for the lowest and highest top shield.

The device used for measuring melt level consists of a depth gauge micrometer with a quartz rod extension ground to a point at the tip. Knowing the distance from the top of the furnace chimney to the top of the susceptor, i.e., the bottom of the lid, one can readily determine the distance between the melt surface and the bottom of the lid to within 0.1 mm by measuring the distance from the top of the chimney to the melt surface and taking the difference between the two values. Similarly, changes in melt level during a run can be accurately determined. Adjustments in melt level to determine the effects of LIN on growth behavior can be made as desired using the melt replenishment system.

3.2.3 Multi-Day Runs

During the course of this reporting period, it has become standard procedure to continue experimental growth runs over a period of two working days, sometimes longer. This procedure greatly increases the amount of information that can be obtained from a given run and simultaneously reduces material costs (crucibles and silicon) and cleaning and set-up time in relation to growing time.

The furnace can be left unattended overnight because of the great thermal stability of the growth system and the ability to control oxide deposition. In addition, time-delayed safety interlocks are included which shut down the system in the event of failure in the water supply or electric power.

3.2.4 Coil Geometry

Through experimental variations of the geometry of induction-heating work coils in web growth furnaces, we have found the front-to-back dimension of the work coil as well as the length-to-width ratio to be an important factor in determining the vertical and lateral

temperature distributions in the susceptor, melt, and lid/shield
stack. This coil shape parameter, in combination with radiation shield
configuration, has been applied to achieve improved temperature profiles
in the newer growth configurations. We have further obtained quantita-
tive information concerning the allowable tolerances in coil dimensions
required to ensure reproducibility between our different growth systems.

3.2.5 Lateral Temperature Distribution

Although the primary requirement for wide web growth is the
generation of the proper vertical temperature profile, the lateral
temperature profile in the lid and shields, as well as the melt, must
also be controlled in order to realize the potential benefits of the
low-stress conditions. Experience suggests that the lateral temperature
distribution is more important for wide ribbons than it is with narrower
ribbons in the 30-35 mm width range, i.e., narrower ribbons are more
forgiving of moderate asymmetries. The thermal requirements of melt
replenishment impose an additional burden on configuring the growth
system for the desired lateral temperature distribution.

The thermal design for producing the desired vertical tempera-
ture profiles is guided by the thermal stress models, but the generation
of the lateral profiles is largely empirical, guided by experience and
experiment. The goal of the lateral temperature trimming is to achieve
a relatively flat and particularly symmetric lateral temperature
distribution in the growth slot region of the lid, shields, and melt.
The means at our disposal include hardware modifications (fixed during a
run) and work coil and end shield positioning (variable during a run).
Assessment techniques include melt profile measurements, shield tempera-
ture measurements and, of course, web growth characteristics such as
buttoning behavior, dendrite smoothness, widening behavior, characteristic
growth velocity, and residual stress.

Experimental data have been collected on the basic J460, the
width-limiting J460L, the J483, and the newer low-stress growth

configurations. The results of this work generated a number of hardware modifications which serve both to generate a relatively flat symmetric lateral temperature distribution in the melt, lid, and shields and to improve the thermal isolation between the growth and replenishment regions of the melt. These modifications included changes in the susceptor shielding, the movable end shields, and the design of the lid/shield stack. In addition, the position of one of the crucible barriers was changed to improve the symmetry.

3.2.6 Achievement of Area Throughput Goals for Transient Growth

Two of the goals of the present program are demonstrations of web growth area throughput rates of 30 and 35 cm^2/min for transient growth. During a portion of this reporting period, experimental web growth was concentrated on achieving these goals.

The growth configuration selected for this work was the J460, a low-stress configuration which has been well characterized. It was carefully thermally trimmed to permit wide high-quality starts and rapid widening, a procedure which consumed most of a three-day run period. This was necessary in order to be able to reach a crystal width at which an attempt at the throughput goals by greatly increasing the pull speed became feasible in a reasonable length of time. Growth system modifications and techniques for optimizing the lateral temperature distributions.

During the next three-day growth period, area growth rates of 32.2 and 32.8 cm^2/min were achieved. In a later run, rates of 29.8 and finally 42.0 cm^2/min were reached. Thus, the area throughput goals for transient growth have been met and exceeded. The experimental results are summarized in Table 2.

These experiments show that web growth is possible at high growth velocity, up to 8 cm/min at widths over 4 cm. The material was, of course, very thin. The configuration used was designed for low stress and improved width, with growth velocity capability being only a

34

37

Table 2

Area Throughput Results

Run No.	Date	Width, cm	Speed, cm/min	Throughput cm^2/min
RE-418	5-19	4.70	6.85	32.2
RE-418	5-20	4.65	7.05	32.8
RE-419	5-26	3.73	8.00	29.8
RE-419	5-27	5.38	7.81	42.0

secondary consideration. These experiments also demonstrated high-quality starts at button widths of 3.5 to 4.0 cm.

3.2.7 Growth Experience with the J460L Configuration

A width control version of the low-stress J460 configuration, designated the J460L, was designed and fabricated. Feed and laser holes for continuous melt replenishment were included in the lids and top shields. These parts were configured so as to prevent oxide accumulation during long duration runs, following the design parameters previously determined and tested empirically. The target steady-state web width for this design was 4 cm, well below the width at which thermal stress-generated buckling would occur in the baseline J460 configuration.

The first run with the J460L was made in the J-furnace with the first and fourth top shields instrumented to provide real temperature data. The growth results were quite encouraging. The first crystal was 5.1 meters long and reached a width of 4.1 cm, consistent with the design goal. The melt was replenished continuously during the last 2.5 hours of growth. During the second day of this run, two additional crystals were grown -- the first to lower the melt, the second with replenishment at a rate somewhat higher than the withdrawal rate -- in order to test growth behavior at different known melt levels. The thickness velocity characteristics and residual stress were also

determined for different melt levels. Although there were some small differences, the general growth behavior of the J460L configuration was consistent with that of the basic J460 design.

Several runs were made with the J460L in the N-furnace with melt replenishment during part of the growth periods. Each run was carried over for a second day. Crystal widths to 4 cm were obtained with growth periods to 3.5 hours. However, growth behavior was not entirely reproducible during these runs, suggesting that shield and coil positions have not been fully optimized.

One run was made with a modified J460 in which the slot width in the lower lid was reduced from 6 mm to 4 mm. The purpose of this run was to verify the prediction of the model that narrowing the slot would enhance growth velocity by reducing the exposure of the web to the hot melt surface. The experimental results did indeed show a small increase in growth velocity and, with minor coil adjustments, good growth, although the physical dimension of the narrow slot required considerable care on the part of the operator during growth initiation.

As this work progressed, the techniques described in Section 3.2.5 were developed and applied to establish the thermal parameters for steady-state growth with the J460L configuration. Several feed stock materials were used in the replenishment experiments. These were cut polysilicon cubes, pellets produced at Westinghouse from the Kayex shot tower, and evaluation samples from an outside supplier. The material supplied from outside was attractive because it was in a form desirable for replenishment feed stock and potentially available in quantity. Preliminary experiments in which it was used as part of the initial charge yielded high-quality web crystals. However, when the material was used for melt replenishment during growth, ice particles were generated at some variable point in time after replenishment was initiated. This time span varied from a few minutes to an hour or more. This behavior was not noticed using the shot tower pellets or cut cubes for replenishment. A run was made in which all three

replenishment materials were alternated; only the outside-supplied
material generated ice specks, even when etched. Therefore, the use of
this material was discontinued.

It should be noted that with the exception of the last run
described above, the purpose of the runs was to evaluate the effects of
variations of furnace parameters and melt level on growth behavior, not
to evaluate replenishment material. Most of the desired data obtained
in runs using different replenishment material were not compromised.
The principal objectives of these experiments, namely to evaluate the
application of newly developed thermal trimming techniques to the J460L
configuration and to define the thermal configuration for continuous
growth with replenishment, were accomplished.

3.2.8 Web Growth With Dynamic Positioning of Thermal Elements

On the basis of a series of parametric studies, it was concluded
that a growth system in which the growth interface-to-lid dimensional
parameter could be dynamically controlled would be a most likely
candidate for providing increased growth. This dimension is identified
as LIN in Figure 8, Section 3.1.4.2. Figure 12 shows a typical
relationship of LIN to the web contribution of the total velocity of web
growth. The web contribution to velocity is one of two components which
comprise the total velocity of web growth and is dependent upon the heat
of fusion which is removed by conduction through the web. The other
component of total velocity is smaller and essentially unrelated to LIN,
and is dependent upon the amount of heat of fusion that is dissipated
into the supercooled melt.

Referring to Figure 5, an apparent mechanism for reducing LIN is
to increase the melt depth by way of the existing melt replenishment
system. This method was performed in laboratory growth and was found to
increase the growth velocity as predicted. The method has,
unfortunately, an intolerable ill effect on web growth. Silicon web
growth inherently requires a very shallow melt in order to minimize

37

41

convective flow and its resultant temperature fluctuations in the melt. When the melt depth was intentionally increased in order to reduce LIN and increase growth velocity, the resulting temperature fluctuations were sufficiently severe to prohibit acceptable web growth.

In order to reduce LIN and to simultaneously maintain a satisfactory melt depth, it was necessary to devise an apparatus and procedure to provide these conditions. Hardware was fabricated and the system was evaluated in experimental web growth, the first run designated RE-421. Tests were designed to compare the new system's performance with the performance of an otherwise identical growth system. The test results demonstrated a major improvement in growth velocity. The velocity at standard thickness (150 um) increased from 1.9 cm/min for the original system to 2.7 cm/min for the new system, a 42% improvement. Details of the new system and its operating procedure will remain unreported pending completion of patent coverage procedure.

A second dynamic design for controlling LIN (RE-431) generated a further improvement in growth velocity to 3-0 cm/min at standard thickness.

Having verified the mechanical function and velocity character-istics, the next dynamic design (RE-435) was an effort to combine the enhanced growth velocity resulting from the dynamic control of LIN with the low-stress characteristics of the J460 design. While we were able to grow with this configuration, considerable effort would be required to optimize it.

3.2.9 New Low-Stress Configuration

Some preliminary experiments were performed with a new low-stress configuration designated the J479, a design which includes a higher shield stack than the J460 configuration. This design was predicted by the models to generate lower buckling stresses than the J460 design. Before this design could be fully evaluated, however, hardware had been fabricated for an even lower stress design, the J483. It did not seem

42

Before this design could be fully evaluated, however, hardware had been fabricated for an even lower stress design, the J483. It did not seem productive at this point to continue working to optimize the intermediate J479 design when the better J483 was available, so experimental work was switched to the latter.

The J483 design is characterized by a significantly higher shield stack than the J460. Preliminary experiments showed that the lateral temperature profiles generated by the new configuration, particularly in the melt, were quite different from those found in the J460 configuration and were not compatible with satisfactory web growth. Simple adjustments such as coil elevation and movable end shield position, were insufficient to generate the desired profiles. The application of some of the techniques discussed in Section 3.2.5 as well as attention to the work coil shape parameter were required to obtain satisfactory profiles. Although some good growth has been obtained, to about 4 cm in width, this configuration has not yet demonstrated the potential predicted by the thermal models because of some growth instabilities not related to stress. Considerable progress has been made in this area and we plan further work with this growth configuration.

Another low-stress growth configuration (J503) was fabricated and tested experimentally. This design is characterized by the incorporation of vertical thermal elements. After some basic adjustments, preliminary results showed easy starting, good lateral temperature distribution in the melt, and stable web growth. However, some modifications on the original design were required in order to bring the temperatures of some of the thermal elements in line with the thermal model. Though not yet optimized, crystals greater than 4 cm wide have been grown with this configuration.

In the course of development of the J483 and J503 configurations, some modifications were made in hardware components in order to provide the three-dimensional temperature distributions needed for stable growth.

43

well-characterized J460 configuration. The result was an improvement in growth and a new maximum undeformed crystal width of 5.8 cm; details are being prepared for "new technology" disclosure.

4. CONCLUSIONS

The thermal models used for analyzing dendritic web growth and calculating the thermal stress were reexamined to establish the validity limits imposed by the assumptions of the models. It would appear that for ribbon width less than about 4 cm, the models give very good results; for much wider widths the models become somewhat conservative. Additionally, the effects of thermal conduction through the gas phase were evaluated and it was found that the contribution was so small that it was inappropriate to include these effects in the model.

New growth designs were generated using the modeling results, and the predicted stress levels were sufficiently small that web crystals in the 6-7 cm width range should be possible. Further, parametric studies indicate that improvement in growth speed should result from dynamic trimming of the LIN parameter, and experimental hardware was fabricated.

More recently, the residual stress effects in dendritic web were examined. This parameter may serve as a diagnostic tool for experimental verification of stress fields near the growth front in much the same way as the buckling behavior evaluates the stress fields further up the ribbon.

Experimentally, new techniques for controlling and fine-tuning temperature distributions in the growth systems have been developed. This work added significantly to our understanding of the interrelation of the details of hardware design and growth behavior, particularly in those aspects of growth not directly related to stress generation. New maximums were achieved in crystal width, growth velocity at standard thickness, area throughput for transient growth, and steady-state growth. These were made possible by our growth in knowledge relating to both the theoretical and implementation aspects of the web growth process.

41

5. PLANS AND FUTURE WORK

Modeling will be continued to improve the low-stress, wide-growth capability of the dendritic web growth configurations. More emphasis will be placed on stress generation near the growth front, and residual stress measurements will be used to evaluate the results of these design improvements. Experimental effort will continue toward implementing the results generated by the models.

6. NEW TECHNOLOGY

A lid design modification of general applicability has been developed which generates improved lateral temperature profiles in the growth region and improved thermal isolation between the growth and replenishment regions of the melt.

A system of growth hardware has been developed for the dynamic positioning of thermal elements to increase the growth rate of silicon dendritic web ribbon.

7. REFERENCES

1. C. S. Duncan et al., Large-Area Sheet Task: Advanced Dendritic Web Growth Development, Annual Report, October 23, 1981 to October 22, 1982, DOE/JPL-955843/83/8, p. 54.

2. Ibid., p. 28.

3. B. A. Boley and J. H. Weiner, Theory of Thermal Stresses (Wiley: New York, 1960), p. 323.

4. C. S. Duncan et al., Large-Area Sheet Task: Advanced Dendritic Web Development, Quarterly Report, April 1, 1981 to June 30, 1981, DOE/JPL-955843/81/3, p. 9.

5. Ibid., p. 11.

6. Ref. 1, p. 13.

7. S. Dushman, Scientific Foundation of Vacuum Technique, 2nd Ed. (Wiley, New York, 1962), p. 42.

8. C. S. Duncan et al., Silicon Web Process Development, Annual Report, April 1978-April 1979, DOE/JPL 954654-79/2, p. 154.

9. Ref. 1, p. 154.

10. S. Timoshenko and D. H. Young, Strength of Materials, 4th Ed. (Van Nostrand, New York, 1962), p. 114.

48

8. ACKNOWLEDGMENTS

Appendix 1
RESIDUAL STRESS MEASUREMENT

Thermal stresses present during the growth of ribbon crystals can cause plastic deformation of the material which is then manifested as a residual stress in the grown material. If a ribbon is obviously deformed, then there must be some level of residual stress present; however, in most cases of dendritic web crystals, the crystal itself shows no macroscopic deformation and the presence of residual stress must be detected by some measurement technique. In the development of dendritic web growth technology, the so-called split-width method has been used to quantify the degree of residual stress present in the grown ribbons. Although such measurements have been made almost from the inception of the program in 1977, very little has been reported on the actual measurement technique. As with any experimental procedure, the proper technique is necessary to achieve reliable results, and it is the purpose of this appendix to document the current practices.

Sample Preparation

For most samples less than about 30 mm wide, a sample strip 20 cm long is used for the stress measurement; for wider samples, there is some indication that a 25 cm long sample may be better. If the residual stresses are large, then the ends of the sample may be distorted and reliable measurements are available only a ribbon width or so away from the ends, and since 20 points or so are desired for the analysis, this dictates a longer strip.

Once the sample strip has been obtained and cleaned of any loose oxide it is placed on a cutting fixture, which is simply a plastic strip narrower than the web so that the bounding dendrities overhang the

46

edges. The strip has a scribed center line and the web is positioned so that the center of the web coincides with the scribed line. Tabs of Scotch tape are convenient for holding the ribbon in position in this and in subsequent operations. Using a plastic straightedge and diamond pencil, the web is then lightly scribed end to end along the centerline. The strip is then removed from the fixture and inverted so that the scribe line is on the bottom and placed on a flat, hard surface. Breaking the sample is accomplished by placing the plastic cutting fixture so that it rests on one dendrite with an edge on the web section approximately over the scribe line. Light pressure on the plastic is then usually sufficient to produce a clean fracture along the length of the sample.

The cutting fixture, which also has cross lines scribed at one centimeter intervals, is now used as the mount for holding the sample for measurement. One of the cleaved strips is taped, scribed side down on the fixture, and the positions of the cross lines roughly indicated by dots made with a fine permanent marker. The matching strip is then positioned so that it coincides as closely as possible with the first strip, especially with regard to alignment of the ends; slight lateral displacements or angular tilt are compensated for in the subsequent analysis. Again, small tabs of tape are used to hold the strips with care being used to avoid any mounting stresses that would compromise the data.

Split-Width Measurement

Actual measurement of the split width is made with a filar eyepiece on a stereoscopic microscope, although the stereoscopic nature of the instrument is not necessary. A very useful feature of the equipment, however, is a continuously adjustable magnification so that the readout of the eyepiece is directly in micrometers (1 div = 1 μm). The split ribbon mounted on the plastic carrier is moved beneath the microscope and measurements are taken every centimeter. The location of the measurement is determined by the cross scribes on the carrier or, if they are not visible, then at the position of the ink dots otherwise used for rough location. In some instances, the quality of the edges of the split strips

47

is not good exactly at the cross scribe, and the measurement is better made at a position as much as a tenth of a millimeter away from the fiducial line. Such an error is negligible in terms of the total x position uncertainty compared with the accompanying y uncertainty (split width).

The uncertainty in the split-width measurement arises from two sources: 1) the uncertainty associated with the definition of the edge of the split and 2) the uncertainty associated with the measurement apparatus. The definition of the edge of the split is to a large extent dependent on the quality of the fracture. If one attempts to measure the separation on the same side as the initial scribe line, then the microchips along the scribe line make it very hard to define the edge. On the opposite side, however, the edge of the fracture is generally sharp and well defined, although care must be taken to be sure that the microscope is well focused on both edges. Even on this side, however, there may be small local regions where there is difficulty in defining the edges; in these cases, the measurement can be made on a closely adjacent region.

The uncertainties associated with the measurement apparatus can be considered to arise from the finite thickness of the lines in the eyepiece reticle. The apparent thickness of the lines is about one division, so the combined uncertainty would be about 1.4 divisions or 1.4 μm at our present magnification. Analysis of a sample of 20 repeated measurements at a single location yielded a standard deviation of 1.26 divisions (μm), in good agreement with rough estimate. It will be shown later that this uncertainty in the individual measurements is generally in good agreement with the uncertainty in fitting the data to the required quadratic form.

Data Analysis

The ultimate parameter that is desired from the analysis of the split-width data is the curvature (or radius of curvature) of one of the segments of the split ribbon. What is calculated is the mean curvature of

48

both segments so that an implicit assumption in the method is symmetry of the system about the center line. Alternatively, the end result of the calculation may be considered as a mean residual stress across the entire ribbon width. A second assumption of the analysis is that the residual stress does not vary along the length of the sample, an assumption that is validated by the observation that the measured residual stress does not vary greatly over ribbon lengths that are much longer than the sample length.

The actual data reduction is simply obtaining a least squares fit of the separation of the ribbon segments, y, and position along the length, x, to the quadratic form

$$y = a_0 + a_1x + a_2x^2.$$ (A-1)

Since the first derivative $y' = a_1$ is generally very small ($<10^{-3}$), the curvature, y'', is easily calculated as $2a_2$ for the total separation, and thus the mean curvature of each segment is simply a_2. Errors in fitting the pieces together are reflected in the other coefficients: a constant separation is reflected in a_0 and an unintentional angular error in a_1; the curvature, a_2, should be relatively unaffected. For example, consider the data shown in Table A-1, which presents the coefficients and their standard errors for repeated measurements on two samples. The final data column in the table is the square root of the mean square deviation for the data points. It can easily be seen that the variation of a_0 and a_1 relative to their uncertainty (standard error) is much larger than the variation of a_2 relative to its standard error. Further, it should be noted that the root of the mean square deviation of the data points from the fitted curve (rmsd) is of the same magnitude in most cases as the uncertainty of the individual split-width measurements, indicating that the data is well represented by the quadratic form of Equation A-1.

53

Table A-1

Coefficients and Their Standard Errors for

Repeated Measurements on Two Samples

Sample	Trial	$10^3 a_o$	$10^4 a_1$	$10^6 a_2$	rmsd(μm)
A	1	0.76 ± 0.11	1.67 ± 0.25	2.07 ± 1.16	1.54
	2	0.97 ± 0.19	2.43 ± 0.42	-0.21 ± 1.96	2.6
	3	1.72 ± 0.23	3.39 ± 0.50	-1.03 ± 2.33	3.1
B	1	1.00 ± 0.13	1.80 ± 0.23	-3.26 ± 0.87	2.0
	2	4.32 ± 0.13	1.67 ± 0.22	-3.35 ± 0.22	1.9

56

FEB 7 1982

FLAT PLATE SOLAR ARRAY PROJECT

Contractor Quarterly, Annual, Interim, and Final
Report Distribution List

Distribution List #645 - Device Measurements and Research Task
(Total = 140 Copies)

	No. of copies		No. of Copies
Applied Solar Energy Corporation Attn: D. C. Leung 15251 East Don Julian Road City of Industry, CA 91746	1	Central Solar Energy Research Corp. Attn: Dr. W. Lance Haworth, PH. D. 328 Executive Plaza 1200 Sixth Street Detroit, MI 48226	1
Arco Solar, Inc. Attn: Library/Aggie Raeder 20554 Plummer Street Chatsworth, CA 91311	1	Comsat General Corp. Attn: Denis Curtin 950 L'Enfant Plaza, SW Washington, DC 20024	1
Arco Solar, Inc. Attn: H. I. Yoo 20554 Plummer St. Chatsworth, CA 91311	1	Cornell University College of Engineering Dept. of Material, Science & Engr. Attn: Dieter G. Ast Ithaca, NY 14850	1
Arizona State University College of Engineering Science Attn: Dr. Charles E. Backus Tempe, AZ 85281	1	Crystal Systems, Inc. Attn: Frederick Schmid Shetland Industrial Park 35 Congress St. Salem, MA 01970	1
Battelle Memorial Institute Columbus Laboratory Attn: Dr. Donald C. Carmichael 505 King Avenue Columbus, OH 43201	1	Dow Corning Corporation Solid State Research Attn: Dr. L. D. Crossman Mail #092 Midland, MI 48640	1
		Dow Corning Corporation Attn: Vishu Dosaj 12334 Geddes Road Hemlock, MI 48626	1
Bell Aerospace Textron Attn: Mr. Frank M. Anthony P. O. Box 1 Buffalo, NY 14240	1	Eaton Corporation Semiconductor Equip. Oper. Nova Implantation Systems Attn: Allen R. Kirkpatrick 16 Tozer Road Beverly, MA 01915	1
Boston College Attn: Dr. P. H. Fang Dept. of Physics Chestnut Hill, MA 02167	1		
Brown University Department of Engineering Attn: Dr. Joseph J. Loferski Providence, RI 02912	1	Electric Power Research Institute Attn: E. A. De Meo 3412 Hillview Avenue P. O. Box 10412 Palo Alto, CA 94304	1

	No. of copies		No. of copies
Electric Power Research Institute Attn: Frank R. Goodman 3412 Hillview Avenue P. O. Box 10412 Palo Alto, CA 94304	1	Kayex Corporation Hamco Division Attn: R. L. Lane 1000 Millstead Way Rochester, NY 14624	1
Energy Materials Corporation Attn: Dave Jewett Ayer Road Harvard, MA 01451	1	Kulicke & Soffa Industries, Inc. Attn: Max Bycer 507 Prudential Road Horsham, PA 19044	1
Exxon Research & Engineering Co. Attn: Dr. James Amick P. O. Box 8 Linden, NJ 07036	1	Lamar University Attn: Dr. Carl L. Yaws P. O. Box 10053 Beaumont, TX 77710	1
General Electric Company Attn: R. N. Hall Corp. R & D P. O. Box 43 Schenectady, NY 12301	1	Arthur D. Little, Inc. Attn: Dr. David Almgren Room 20-531 Acorn Park Cambridge, MA 02140	1
GHS Consulting Attn: Dr. G. H. Schwuttke 6 Spur Way Ponghkeepsie, NY 12603	1	Massachusetts Institute of Tech. Lincoln Laboratory Attn: Mr. Marvin Pope Room I-210 244 Wood Street or (P. O. Box 73) Lexington, MA 02173	1
Honeywell, Inc. Corporate Technology Center Attn: J. D. Heaps 10701 Lyndale Avenue South Bloomington, MN 55420	1	Dr. H. F. Matare P. O. Box 49177 Los Angeles, CA 90049	1
Jet Propulsion Laboratory Attn: (Contract Negotiator) M/S 511-303 4800 Oak Grove Drive Pasadena, CA 91109	1	Materials Research, Inc. Attn: Dr. Ram Natesh 790 East 700 South Centerville, UT 84014	1
Jet Propulsion Laboratory Attn: Solar Data Center M/S 502-414 4800 Oak Grove Drive Pasadena, CA 91109	35	Mobil Tyco Solar Energy Corp. Attn: K. V. Ravi 16 Hickory Drive Waltham, MA 02154	1
Jet Propuslion Laboratory Technology Utilization Attn: L. P. Speck M/S 180-302 4800 Oak Grove Drive Pasadena, CA 91109	1	Mobil Tyco Solar Energy Corp. Attn: Fritz Wald 16 Hickory Drive Waltham, MA 02154	1
		Monegon, Ltd. Attn: Scott Kaufman 4 Professional Drive Suite 130 Gaithersburg, MD 20760	1

56

	No. of copies		No. of copies

Monsanto Research Corporation — 1
Attn: H. Gutsche
P. O. Box 8
St. Peters, MO   63376

National Science Foundation — 1
Division of Applied Research
Attn: Dr. Tapan Mukherjee
1800 G. Street N.W.
Washington, DC   20550

Motorola, Inc. — 1
Semiconductor Group
Attn: R. Gurtler
5005 East McDowell Road
Phoenix, AZ   85008

Photon Power — 1
Attn: C. Lampkin
10767 Gateway West
El Paso, TX   79935

Motorola, Inc. — 1
Semiconductor Group
Attn: I. Arnold Lesk A-110
5005 East McDowell Road
Phoenix, AZ   85008

RCA, Advanced Technology Labs. — 1
Attn: M. S. Crouthamel
Building 10-8
Camden, NJ   08102

NASA Headquarters — 1
Solar Terr. Systems Div.
Attn: John Loria
600 Independence Ave., SW
Washington, DC   20546

RCA, Laboratories — 1
David Sarnoff Research Center
Attn: Arthur Firester
Princeton, NJ   08540

NASA Headquarters — 1
Attn: J. P. Mullin, Code RP-6
       M/S B636
Washington, DC   20546

Rockwell International — 2
Electronics Research Center
Attn: Dr. R. P. Ruth
       D/540, HA32
3370 Miraloma Avenue
Anaheim, CA   92803

NASA Lewis Research Center — 5
Photovoltaic Project Office
Attn: William Brainard
       M/S 49-5
21000 Brookpark Road
Cleveland, OH   44135

Rockwell International — 1
Energy System Group
Attn: Mr. B. L. McFarland
       Dept. 714
8900 Desoto Ave.
Canoga Park, CA   91304

NASA Lewis Research Center — 1
Attn: Dr. John C. Evans Jr.
       M/S 302-1
21000 Brookpark Road
Cleveland, OH   44135

Bernd Ross Associates — 1
Attn: Dr. Bernd Ross
2154 Blackmore Court
San Diego, CA   92109

National Bureau of Standards — 1
Attn: Sam R. Coriell
       B164 Matls.
Washington, DC   20234

C. T. Sah Associates — 1
Attn: Dr. C. T. Sah
403 Pond Ridge Lane
Urbana, Il   61801

National Bureau of Standards — 1
Attn: David E. Sawyer
Bldg. 225, Room B-310
Washington, DC   20234

Semix Inc. — 1
Attn: Thomas Rosenfield
15809 Gaither Road
Gaithersburg, MD   20760

57

	No. of copies		No co

Silicon Technology Corporation   1
Attn: Dr. George S. Kachajian
P. O. Box 310
48 Spruce Street.
Oakland, NJ   07436

Siltec Corporation   1
Attn: R. E. Lorenzini
3717 Haven Avenue
Menlo Park, CA   94025

Solamat, Inc.   1
Attn: Dr. Barton Roessler
885 Watermann Ave.
East Providence, RI   02914

Solar Energy Research Institute   1
Attn: Dr. Charles J. Bishop
1617 Cole Blvd.
Golden, CO   80401

Solar Energy Research Institute   1
Attn: SEIC/LIBRARY
1617 Cole Blvd.
Golden, CO   80401

Solar Energy Research Institute   1
Attn: Gary Nuss
1617 Cole Blvd.
Golden, CO   80401

Solar Energy Research Institute   1
Photovoltaic Branch
Attn: Ted Ciszek
1617 Cole Blvd.
Golden, CO   80401

Solar Energy Research Institute   1
Photovoltaic Program Office
Attn: D. W. Ritchie
1617 Cole Blvd.
Golden, CO   80401

Solar Energy Research Institute
Photovoltaic Program Office
Attn: Dr. Tom Surek
1617 Cole Boulevard
Golden, CO   80401

Solar Energy Research Institute
Photovoltaic Program Office
Attn: Dr. C. Edwin Witt
1617 Cole Blvd.
Golden, CO   80401

Solar Energy Systems
Attn: W. J. Kaszeta
One Tralee Industrial Park
Newark, DE   19711

Solar Power Corporation
Attn: P. Caruso
20 Cabot Road
Woburn, MA   01801

Solarex Corporation
Attn: John V. Goldsmith
1335 Piccard Drive
Rockville, MD   20850

Solarex Corporation
Attn: Dr. Joseph Lindmayer
1335 Piccard Drive
Rockville, MD   20850

Solec International, Inc.   1
Attn: Ishaq Shahryar
12533 Chadron Avenue
Hawthorne, CA   90250

Southern Methodist University
Institute of Technology
Electrical Engineering Dept.
Attn: T. L. Chu
Dallas, TX   75275

Spectrolab, Inc.   1
Attn: Dr. J. Minahan
12500 Gladstone Avenue
Sylmar, CA   91342

58

	No. of copies		No. of copies

Spectrolab, Inc.   1
Attn: E. L. Ralph
12500 Gladstone Avenue
Sylmar, CA   91342

Underwriters Laboratories   1
Attn: Al Levins
1285 Walt Whitman Road
Melville
Long Island, NY   11746

Spire Corporation   1
Patriots Park
Attn: R. Little
P. O. Box D
Bedford, MA   01730

Underwriters Laboratories   1
Attn: William J. Christian
333 Phingsten
Northbrook. IL   60062

Stanford Research Institute   1
Materials Research Center
Attn: Dr. Angel Sanjurjo, G213
333 Ravenswood Avenue
Menlo Park, CA   94025

Union Carbide Corporation   1
Linde Division
Attn: Dr. Hiroshi Morihara
P. O. Box 44
Tonawanda, NY   14150

Stanford University   1
Center for Materials Research
Attn: Dr. Robert S. Feigelson
Stanford, CA   94305

State University of New York   1
College of Engineering
Department of Materials Science
Attn: Dr. Franklin F. Y. Wang
Stony Brook, NY   11794

University of Delaware   1
Dept. of Electrical Engr.
Attn: Allen M. Barnett
Newark, DE   19711

University of Illinois   1
Materials Engineering
Chicago Circle Compus
Attn: Steven Danyluk
Chicago, IL   60680

Strategies Unlimited   1
Attn: Dough Finch
    Suite 205
201 San Antonio Circle
Mountain View, CA   94040

University of Pennsylvania   1
Attn: Prof. Martin Wolf
308 Moore D2
Philadelphia, PA   19174

Texas Instruments, Inc.   1
Semiconductor Group
Attn: Dr. L. D. Dyer
    M/S 960
P. O. Box 225621
Dallas, TX   75265

U. S. Airforce   1
Air Force Aeropropulsion Lab.
Attn: Mr. Joseph Wise
AFAPL/POE-2
Wright-Patterson AFB, OH   45433

Tideland Signal Corp.   1
Attn: Mr. Carl Kotilla
P. O. Box 52430
Houston, TX   770521

U. S. Army/MERADCOM   1
Attn: DRDME-E/Mr. Donald D. Faehn
Fort Belvoir, VA   22060

TRW Systems Group   1
Attn: Paul Goldsmith
    Bldg. M1/1334
One Space Park
Redondo Beach, CA   90278

U. S. Department of Energy   1
Forrestal Building
Attn: Mr. Alan Postlehwaite
1000 Independence Ave., SW
Washington, DC   20585

59

	No. of copies

U. S. Department of Energy   1
Forrestal Building
Attn: Dr. Morton Prince M/S 5G026
Photovoltaic Energy Systems
1000 Independence Ave., SW
Washington, DC   20585

U. S. Department of Energy   2
Technical Information Center   + Repro
Attn: Doc. Control & Eval. Branch
P. O. Box 62
Oak Ridge, TN   37830

Virginia Semiconductor, Inc.   1
Attn: Dr. Thomas G. Digges, Jr.
1501 Powhatan St.
Fredericksburg, VA   22401

Western Electric   1
Semiconductor Materials Engineering
Attn: R. E. Reusser - 6510
555 Union Boulevard
Allentown, PA   18103

Westinghouse Electric Corporation   1
Research Laboratories
Attn: C. Duncan
1310 Beulah Road
Pittsburgh, PA   15235

Westinghouse Electric Corporation   1
Research Laboratories
Attn: R. H. Hopkins
1310 Beulah Road
Pittsburgh, PA   15235

Westinghouse Electric Corporation   1
Advanced Energy Systems Division
Attn: Dr. P. F. Pittman
P. O. Box 10864
Pittsburgh, PA   15236

Westinghouse Electric Corporation   1
Research Laboratories
Attn: Dr. P. Rai-Choudhury
1310 Beulah Road
Pittsburgh, PA   15235

	No. of copies

Westinghouse Electric Corporation   1
Research Laboratories
Attn: R. K. Riel
1310 Beulah Road
Pittsburgh, PA   15235

Westinghouse Electric Corporation   1
Research Laboratories
Attn: Dr. R. G. Seidensticker
1310 Beulah Road
Pittsburgh, PA   15235

Dr. Robert J. DeAngelis
Dept. of Metallurgical Engineering
University of Kentucky
Lexington, KY 40506